Physical and chemical properties of PAN-derived electrospun activated carbon nanofibers and their potential for use as an adsorbent for toxic industrial chemicals

P. Sullivan · J. Moate · B. Stone · J.D. Atkinson · Z. Hashisho · M.J. Rood

Abstract A recently developed carbon material, electrospun Activated Carbon nanoFiber (ACnF), exhibits strong potential for use as an adsorbent for toxic industrial chemicals (TICs). As-prepared ACnF contains as much as 9.6 wt% nitrogen, creating a basic surface that enhances acid-gas adsorption. ACnF shows 4–20 times greater HCN adsorption capacities and 2–5 times greater SO_2 adsorption capacities in dry nitrogen, compared to commercially available activated carbon fiber cloth (ACFC) and Calgon BPL™ granular activated carbon, which are considered here as reference adsorbents. ACnF has 50 % of the micropore volume (0.30 cm^3/g) of these reference adsorbents, which limits its adsorption capacity at high concentrations for volatile organic compounds (>500 ppm$_v$). However, at low concentrations (<500 ppm$_v$), ACnF has a similar capacity to ACFC and about three times the VOC adsorption capacity of Calgon BPL™. ACnF's small fiber diameters (0.2–1.5 μm) allow for higher mass transfer coefficients, resulting in adsorption kinetics nearly twice as fast as ACFC and eight times as fast as Calgon BPL™. ACnF drawbacks include hydrophilicity and reduced structural strength. The rapid adsorption kinetics and high capacity for acidic TICs warrant further investigation of ACnF as an adsorbent in respiratory protection and indoor air quality applications.

P. Sullivan · J. Moate
Air Force Research Laboratory, 139 Barnes Dr. Suite 2, Tyndall AFB, FL 32403, USA

B. Stone
Applied Research Associates, 421 Oak St., Panama City, FL 32401, USA

J.D. Atkinson · M.J. Rood (✉)
University of Illinois, Urbana, IL 61801, USA
e-mail: mrood@illinois.edu

Z. Hashisho
University of Alberta, Edmonton, AB T6G 2M7, Canada

1 Introduction

Improved sorbents are desirable to increase performance (e.g., selective adsorption capacities and mass transfer kinetics) and reduce the weight, size, and power consumption of gas purification systems. In the military, where many of the gas purification systems are mobile (e.g., vehicles, transportable shelters, respirators), reducing the physical or logistical burden of these systems is of particular importance.

Increased use of asymmetric warfare tactics in recent years emphasizes the need to provide protective filtration against both conventional chemical warfare agents and a wide variety of toxic industrial chemicals (TICs) that could be used as improvised weapons. For example, terrorists used chlorine gas in association with explosive devices in Iraq during 2007 (Weitz et al. 2007).

Military adsorbents have traditionally been carbon-based. Activated carbon is well suited to capturing organic compounds, including many chemical warfare agents (CWAs), in an uncontrolled (often humid) environment. Activated carbons can be hydrophobic and have high micropore volume (relative to zeolites), are thermally stable, and are resistant to degradation in both acidic and basic environments (relative to metal–organic frameworks) (Rodriguez-Reinoso 1998).

However, not all TICs and CWAs are strongly adsorbed onto conventional activated carbon, and adequate protection cannot be achieved by physisorption alone. Impregnants or chemical surface functionalities can be added to the

carbon, modifying its pH, polarity, and reactivity, to target specific contaminants and enhance physisorption or induce chemisorption and/or other surface reactions (e.g., catalysis, (Bansal and Goyal 2005)).

Impregnation of carbon adsorbents has advantages and disadvantages. Chemical impregnants are added to the bulk and surface of a carbon, often through excess solution or incipient wetness impregnation techniques, and are not chemically bound to the carbon. When compatible, multiple impregnants can be employed to address a wide spectrum of adsorbates with a single adsorbent. Impregnation, however, decreases carbon's accessible porosity and surface area by partially filling or occluding pores, potentially limiting the material's capacity for contaminants. Impregnants can also age (i.e., migrate, agglomerate, or react over time), decreasing their effectiveness (Brown et al. 1989). Impregnated adsorbents cannot be regenerated to initial capacity by thermal or pressure swing if the impregnants are consumed during use. A popular impregnated carbon used for military applications is Calgon AZSM-TEDA, which is impregnated with copper, silver, zinc, molybdenum, and triethylenediamine (TEDA) (Peterson and Karwacki 2007). TEDA makes the carbon basic, enhancing capture of acidic TICs.

Unlike chemical impregnants, surface functionalities are covalently bound to the carbon adsorbent, increasing stability and the likelihood of reversible complexation or chemisorption, and minimizing aging effects. Employing an adsorbent material that relies on physisorption or reversible chemisorption mechanisms enables an adsorption process to be cyclical, allowing off-line regeneration and reuse of devices such as respirator cartridges. Reversibility also affords the opportunity for automated, continuous-duty operation of multi-vessel collective protection systems. For these reasons, an adsorbent based on chemical surface modification, rather than impregnation, is desirable, if sufficient protection can be achieved. Surface functionalities may be formed by using specific precursor materials or additives in the carbonization/activation process or by high-temperature, post-activation processing. Numerous processes have been used to modify carbon surface chemistry both experimentally and commercially (Rivera-Utrilla et al. 2011). Acidic functional groups (i.e., –COOH) can be added by oxidation of the carbon with acids, peroxides, or ozone. Oxidized activated carbons have demonstrated improved performance for capturing ammonia (Mangun et al. 1999). The degree of oxidation of carbons to produce the desired –COOH functional groups should be carefully controlled, as oxidation can result in loss of pore volume, reduced surface area, and an increase in mean pore size, through destruction of pore walls (Pradhan and Sandle 1999; Pereira et al. 2003; Sullivan et al. 2007).

Basic functional groups (e.g., amine, pyridine) on carbon have been produced by post-activation treatment with ammonia, urea, or melamine, or by using a nitrogen-containing activated carbon precursor material such as polyacrylonitrile (PAN) (Song et al. 2008). Improved performance in capturing SO_2 (Mangun et al. 2001b; Bagreev et al. 2002), HCl (Mangun et al. 2001a), and H_2S (Boudou et al. 2003) has been documented for carbons treated with ammonia. Addition of basic functional groups to carbon's surface via nitrogen impregnation is a complex process, as retaining the nitrogen, which can exist in numerous forms—many of which are not basic (e.g., pyrrole)—in the carbon structure can be difficult. Some general trends can be discerned from the literature on producing basic, nitrogen-functionalized carbons:

1. The higher the processing temperature, the less nitrogen that is retained in the structure (Ko et al. 1992; Ryu et al. 2002). This trend is counter to the increase in porosity, so these two concerns must be balanced.
2. Higher nitrogen content can be obtained when the nitrogen is added to the carbon during carbonization/pyrolysis rather than during activation or post-treatment processing (Mangun et al. 2001b; Yue et al. 2002). This is reasonable, as the desired pyridine structures are more easily produced during ring formation, which occurs during carbonization.
3. Acid-gas capture capacity is proportional to the bulk nitrogen content of the adsorbent (Economy and Mangun 2002; Song et al. 2008).

Herein, we report the physical, chemical, adsorptive, and adsorption kinetic properties of a recently developed PAN-derived Activated Carbon nanoFiber (ACnF) adsorbent produced by electrospinning and subsequent carbonization and activation, and compare the properties of this adsorbent to commercially available activated carbon fiber cloth (ACFC) and Calgon BPL™ granular activated carbon (GAC)

2 Methods

2.1 Precursor selection and nonwoven nanofiber material preparation for ACnF

A PAN-based copolymer was synthesized as the precursor for ACnF at eSpin Technologies, Inc., of Chattanooga, TN. The polymer composition was optimized for molecular weight and composition to enhance the desired properties of the end product ACnF. The electrospinning parameters included a potential of 28 kV and a distance from the ejector to the target of 5.1 cm (Vora 2009). The precursor polymer was electrospun into a nanofiber web resulting in fiber diameters mainly in the 200–500 nm range, but a few larger fibers are also observed.

2.2 Carbonization and activation of ACnF

The resulting PAN-based nanofiber web was pyrolyzed and activated to obtain the desired degree of activation. The thermal processing consists of stabilization in air, carbonization in an inert atmosphere, and activation using CO_2. The heating profile and soak times were determined by thermogravimetric analysis/differential scanning calorimetry (TGA/DSC) (Vora 2009).

2.3 Reference adsorbent materials

Reference adsorbents selected for comparison to ACnF include Calgon Carbon Corporation's BPL™ granular activated carbon (GAC) and American Technical Trading, Inc. ACFC (ACC-5092-15). The GAC was a standard 12×30 mesh with a bulk density of 0.49 g/cm^3. The ACFC is available in different degrees of activation, with ACC-5092-15 representing a "medium" level of activation.

2.4 Scanning electron microscopy and bulk physical properties

Scanning Electron Micrographs (SEMs, Hitachi S4700) were obtained at the University of Illinois' (UI) Center for Microanalysis of Materials. Samples were prepared by loading the carbon materials onto carbon tape located on an aluminum disk. The disk was loaded into the sample chamber where it was analyzed at low total pressures (<1 Pa). Accelerating voltages of 10–15 kV were used for all images presented in this study. Areal density and electrical resistivity of the ACnF were measured using methods previously described for ACFC (Sullivan et al. 2001).

2.5 N_2 adsorption isotherms

N_2 adsorption isotherms were generated volumetrically (Micromeritics, Inc., Model ASAP 2010). Samples were degassed for >6 h at 150 °C under at 4–6 mm Hg. The adsorption isotherms were obtained at 77 K and $10^{-6} < P/P_0 < 0.99$. The Brunauer, Emmett, and Teller (BET) method was used to fit the adsorption data from $0.06 < P/P_0 < 0.20$. Micropore volume and pore size distribution were determined using the 3-D Model (Sun et al. 1998). The average micropore width was determined for pore widths ≤ 20 Å, and the total pore volume was determined at $P/P_0 = 0.99$ using the bulk liquid density for N_2 (0.808 cm^3/g).

2.5.1 X-ray photoelectron spectroscopy (XPS) and elemental analysis

The surface elemental composition of select carbons was determined using XPS (PHI 5400, Perkin–Elmer, Physical Electronics Inc.; and Kratos Axis Ultra), at the UI Center for Microanalysis of Materials. For the PHI 5400, an area of 1 mm^2 was targeted with Mg Kα or Al Kα radiation at a power of 300 W at 15 kV under ultrahigh vacuum (10^{-8} to 10^{-9} torr). For the Kratos Axis Ultra, Mg Kα radiation was used. The Kratos instrument provides elemental composition (excluding hydrogen) with 0.1 % sensitivity. Elemental compositions determined by XPS are reported as percents relative only to the elements being measured.

For select samples, data obtained using the Kratos Axis Ultra instrument was analyzed further using CasaXPS software to determine the identity and distribution of nitrogen functionalities. The C1s peak was adjusted to 284.5 eV before fitting the N1s peak. Nitrogen peak models were generated using the CasaXPS software, assuming Gaussian-shaped peaks.

Bulk carbon, hydrogen, nitrogen (CHN) analysis was performed at the UI Chemistry Microanalysis Lab with a CE-400 Elemental Analyzer by Exeter Analytical, Inc., that combusts the sample in pure oxygen at 980 °C. CO_2, H_2O and N_xO_y are detected in a series of traps and thermal conductivity cells. Oxygen in the sample is determined by mass difference—causing adsorbed water contamination to appear as excess oxygen. However, effort was taken to dry the samples and limit their exposure to the atmosphere before completing the elemental analysis. The instrument has a detection limit of 0.10 % and error of 0.06 % for all measured elements. As with XPS, elemental compositions determined by CHN are reported as percents relative only to the elements being measured.

2.6 Gravimetric adsorption isotherms

H_2O, SO_2, HCN, and butane adsorption/desorption isotherms were obtained gravimetrically (Model GHP-F and Model SGA-100 of VTI Corporation of Hialeah, FL, now TA Instruments of New Castle, DE). The GHP-F system uses a magnetic suspension balance (Rubotherm of Bochum, Germany). Mass flow controllers are used in both systems to proportion flow between the adsorbate gas and a nitrogen carrier gas to achieve desired concentrations.

For water adsorption isotherms, an evaporator produced a fully humidified gas stream for proportioning. For HCN, SO_2, and n-butane, a gas cylinder of a certified concentration (in ultra-high purity nitrogen) was used as purchased from Air Liqude America Specialty Gases.

Each carbon sample was dried at 200–250 °C at atmospheric pressure under nitrogen prior to generating the adsorption isotherm, until a static weight was achieved (<0.03 % change in 10 minutes) or for a maximum time of 1 h. Carbon samples ranged from 40 mg to 150 mg in the GHP-F, and 30 mg to 60 mg in the SGA-100.
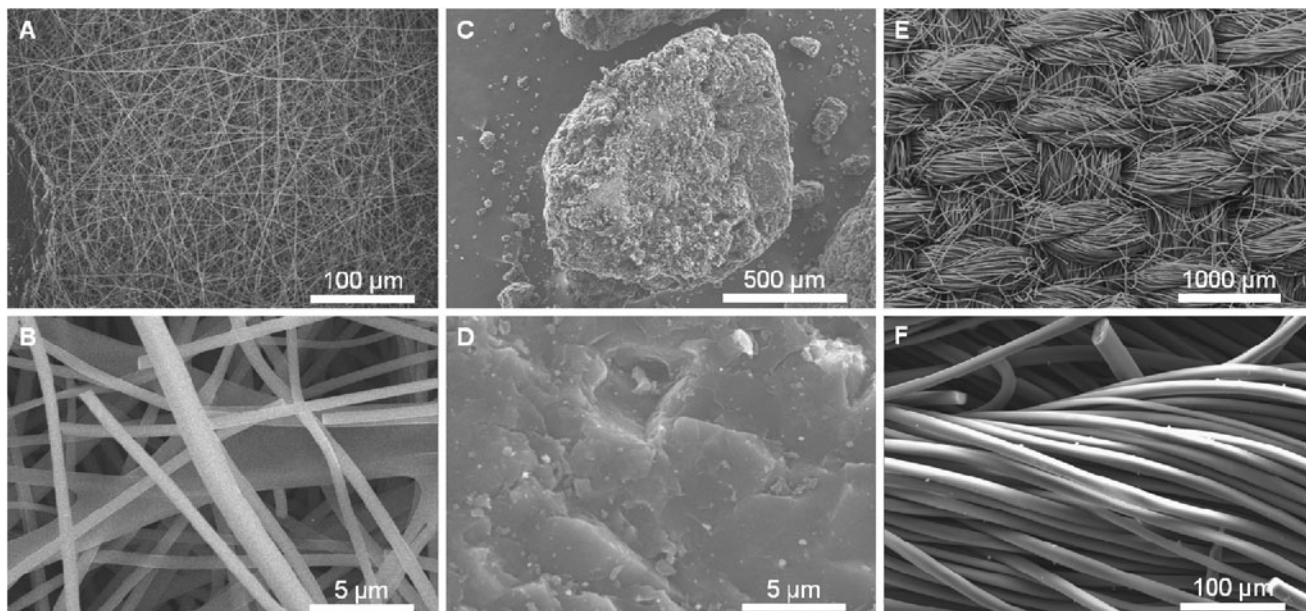
Fig. 1 SEM images of ACnF (**A**, **B**) showing filament arrangement, shape, and texture with comparisons to the reference BPL™ (**C**, **D**) and ACFC (**E**, **F**)

2.7 Gravimetric kinetic measurements

During gravimetric equilibrium isotherm experiments, quantitative kinetic data were collected for ethane (using a certified 5000 ppm$_v$ cylinder). After each step change in concentration, the adsorbent exponentially approached a new equilibrium weight. Adsorption data of this type may be modeled by Avrami's Equation (Calvete et al. 2009):

$$q_t = q_e\{1 - \exp[-k_{AV}t]^{n_{AV}}\} \tag{1}$$

where q_t is the mass loading at time t, q_e is the equilibrium mass loading, and k_{AV} and n_{AV} are the Avrami coefficient and exponent, respectively. Software provided with the GHP-F and SGA-100 analyzers performs a similar kinetic analysis, assuming $n_{AV} = 1$, and determines k_{AV} for the specified equilibrium step. This is equivalent to assuming a pseudo-first-order kinetic model (Azizian 2004). The time to reach equilibrium depends on the adsorbate–adsorbent system, temperature, step change in concentration, and fractional loading relative to saturation. The kinetic measurements for each adsorbent were collected with the same adsorbate and similar concentrations, temperature, concentration step change, and fractional loadings to ensure consistency. The intent here is only to provide a comparative screening of the kinetics of this new nano-structured material that might serve as the impetus for further studies. Ethane was used for kinetic experiments to minimize rate variation related to pore filling.

Table 1 Physical properties of fibrous adsorbents

Material	Thickness (uncompressed) (mm)	Thickness (compressed) (mm)	Areal density (g/m^2)	Electrical resistivity (ohm-cm)
ACnF	0.09	0.05	12.4	0.484
ACFC	0.61	0.48	180	0.202[A]

[A] (Sullivan et al. 2001)

3 Results and discussion

3.1 Materials characterization

SEMs of ACnF reveal a mat of randomly arranged long, linear fibers (Fig. 1A–B). Fibers are cylindrical, smooth, and have diameters of 0.2–1.5 μm. BPL$_{TM}$ granules have a large diameter (∼1 mm) and a rough and flaky surface morphology (Figure 1C–D). ACFC consists of systematically woven fibers with diameters of 10–15 μm, between one and two orders of magnitude larger than ACnF (Fig. 1E–F).

The random arrangement of the fibers in ACnF (Fig. 1A) results in a lower areal density than ACFC (Fig. 1E), which has organized, tightly packed yarns (Table 1). It is expected that the bulk of this difference in density is accounted for with spacing between the fibers, as opposed to porosity developed within the individual fibers during activation, as it is later shown that ACFC has more total pore volume than ACnF. Qualitatively, ACnF could be described as similar in appearance and texture to facial tissue, while ACFC is akin to the fabric in a woven cloth.

Table 2 Summary of surface areas and pore size distributions for ACnF, BPL™ and ACFC

Property	ACnF	BPL™	ACFC
Total pore volume (cm³/g)	0.30	0.53	0.64
Micropore volume (cm³/g)	0.30	0.47	0.64
Microporosity (%)	100	89.0	99.8
Average micropore width (Å)	7.2	8.7	7.7
BET surface area (m²/g)	693	942	1,262

The impacts of activated carbon's physical and chemical properties on its electrical resistivity are not well understood. Limited data has been published on the electrical resistivity of fibrous activated carbon materials (Nakayama et al. 1996; Subrenat et al. 2001; Sullivan et al. 2001; Luo et al. 2006). For granular systems, the contact resistance between individual carbon granules has been shown to be a significant component of the overall electrical resistance of an adsorbent bed (Saysset 1999), and to be inversely proportional to the mechanical pressure at the contact points. The random arrangement of the individual carbon nanofibers in ACnF may increase the distance through which current must travel along individual carbon fibers, as well as increase the number of contact junctions that must be traversed, as compared to the woven ACFC. These factors might explain why ACnF has a higher electrical resistivity than ACFC, although a detailed analysis of the electrical properties of these materials is beyond the scope of this work.

ACnF has less total surface area and micropore volume and narrower micropore widths than the two reference materials (Table 2). From the upward sloping center section of its N_2 adsorption isotherm, BPL can qualitatively be seen to have a wider pore distribution that includes mesopores (Fig. 2). The adsorption isotherms for the fibrous media plateau more rapidly, ACFC having slight mesoporosity, and ACnF exhibiting no discernable mesoporosity (Fig. 2, Table 2). It is probable that ACnF is activated to a lesser degree than ACFC, supported by its lower surface area and total pore volume. Micropore size distributions for the three selected carbons are described in Fig. 3.

Surface and bulk elemental compositions reveal that ACFC and BPL™ are predominantly carbonaceous, with a small percentage of oxygen, reflective of some surface oxidation (Table 3). ACnF contained 7–10 % nitrogen on the surface and in the bulk, significantly more than either ACFC or BPL™. Nitrogen content in ACnF is expected when using the polyacrylonitrile (PAN) precursor and activation with CO_2 (Wang et al. 1996). It has been shown that nitrogen is eliminated from PAN-based precursors during activation, and that this elimination is enhanced when steam activation is used (Wang et al. 1996). It follows, therefore, that the ACnF is a less activated material than the other commercial activated carbons, as was also postulated based on the
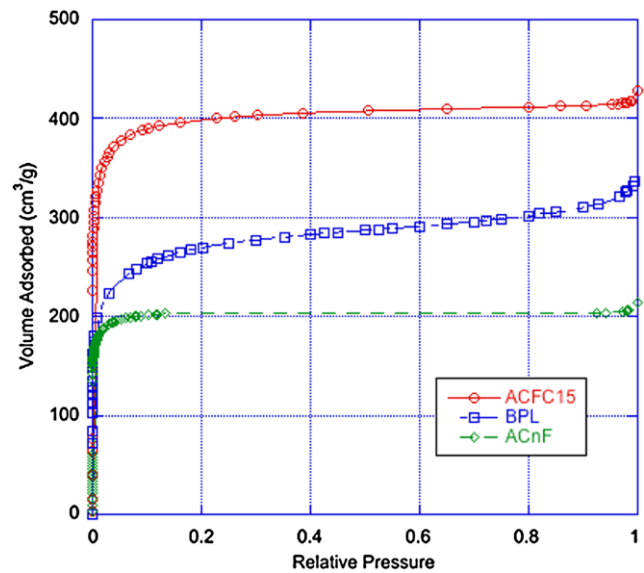
Fig. 2 N_2 adsorption isotherms at 77 K of ACnF, ACFC, and BPL™
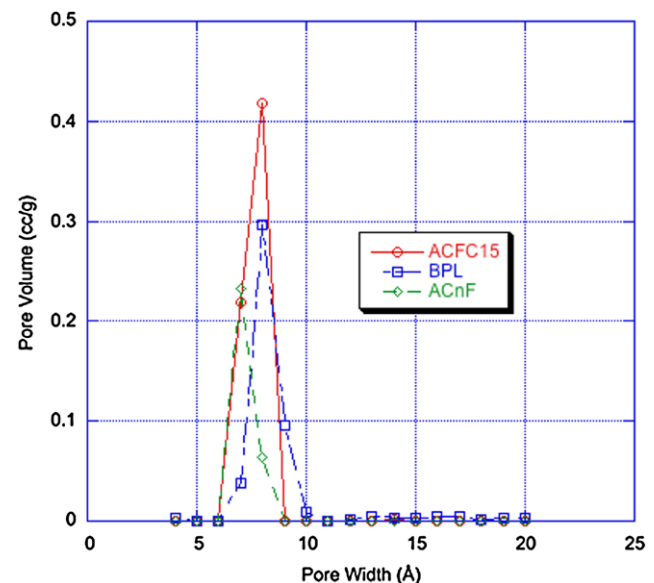
Fig. 3 Micropore size distribution of ACnF, BPL™, and ACFC by the 3-D model (Sun et al. 1998)

material's physical properties. The bulk nitrogen content of ACnF is twice that observed in other commercially available PAN-derived carbon fibers, 3–4 times that of rayon-derived carbon fibers, and nearly 20 times that of novoloid-derived ACFC (Chiang et al. 2007). The nitrogen content of untreated ACnF is similar to the highest levels achieved by activation of Kynol™ phenolic resin in ammonia (Mangun et al. 2001a).

ACnF contained similar levels of oxygen as BPL™ on the surface and in the bulk, and more than ACFC. These levels of nitrogen and oxygen increase the polarity of the ACnF and result in increased hydrophilicity compared to the

Table 3 Elemental analysis of activated carbons

Bulk analysis (CHN) material	Carbon (%)	Nitrogen (%)	Hydrogen (%)	Oxygen (%)
ACnF	81.8	6.5	1.40	10.3
BPL™	89.2	0.8	0.07	9.9
ACFC	95.1	0.4	0.6	3.9

Surface analysis (XPS[A]) material	Carbon (%)	Nitrogen (%)	Hydrogen[B] (%)	Oxygen (%)
ACnF	85.8 (84.7)	6.9 (9.6)	ND	7.3 (5.0)
BPL™	93.3	0.4	ND	6.3
ACFC	95.4 (94.6)	0 (1.4)	ND	4.5 (3.9)

[A] XPS data between parentheses were obtained with a PHI5400 system; XPS data without parentheses were obtained with a Kratos system
[B] ND: Not detectable with XPS
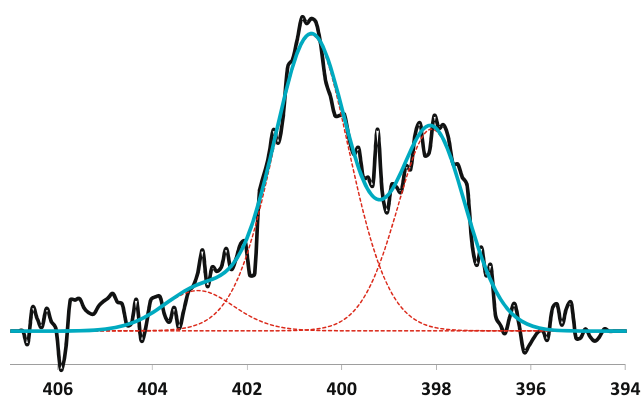
Fig. 4 N1s spectra for ACnF with corresponding peak model (Residual Standard Deviation = 0.71)

Table 4 Speciation of N-containing functional groups in ACnF

Peak location (eV)	Relative concentration (%)	Peak identity
398.1	35.4	Pyridinic
400.7	57.3	Pyrrolic
403.1	7.3	Pyridine-N-oxide

ACFC. The coal-derived BPL™ has been measured to contain a significant amount of ash at 6.3 % (Evans et al. 1998), while the carbons from synthetic precursors generally contain a much smaller amount, perhaps less than 1 %. An insufficient quantity of the ACnF was available to measure this property with reproducibility. ACFC is ash free (Ramirez et al. 2004).

XPS was used to identify nitrogen functional groups on the surface of ACnF (Fig. 4, Table 4). Peaks were identified by comparing XPS peak binding energies to the literature. Boudou showed that treatment of viscose-based carbon fibers with gaseous ammonia resulted in approximately twice as many pyridinic functionalities as pyrrolic functionalities (Boudou 2003). Others have shown similar results for ammonia-treated carbons (Stohr et al. 1991; Mangun et al. 2001a; Kundu et al. 2010). ACnF, however,

contains nearly twice as many pyrrolic functionalities as pyridinic functionalities, with a small component of pyridine-N-oxide (Table 4). Pyrrolic groups are less basic than pyridinic groups, but the still significant pyridine component of ACnF should render the carbon quite basic. Pyrrolic and pyridinic functionalities on carbon materials have similar thermal stabilities, with non-catalytic evolution of nitrogen-containing gases not starting until 500 °C (Wu et al. 2003).

3.2 Gravimetric adsorption isotherms

n-Butane (boiling point −42.1 °C) was selected as a probe molecule for the carbon materials as it is nonpolar and is physisorbed by activated carbons. Also, the isotherm of n-butane is informative in the concentration range of interest (0–5,000 ppm$_v$) for TIC adsorption. At lower concentrations, the activity of high-energy pores is revealed, and at higher concentrations pore filling is observed, up to ∼1/3 of the total pore volume. ACnF adsorbs 55 % and 25 % less n-butane than ACFC and BPL™ at high adsorbate concentrations (i.e., 4,500 ppm$_v$ n-butane), respectively (Fig. 5). At low n-butane concentrations (<500 ppm$_v$), however, ACnF performs quite similarly to ACFC and about three times better than Calgon BPL™. This is expected because adsorption of n-butane at high concentrations is controlled by the total pore volume of the adsorbent, adsorbate–adsorbate interaction, and adsorbate–adsorbent interaction. At low concentrations, adsorption is controlled only by adsorbate–adsorbent interactions. These interactions are favored in adsorbents with narrower pores and more surface functional groups, as is the case of ACFC and, in particular, ACnF. ACnF's relatively low adsorption capacity for n-butane at elevated concentrations results from the low total micropore volume of ACnF compared to ACFC and BPL™. Additional activation of ACnF would increase its capacity for n-butane at high concentrations by increasing the total pore volume and/or surface area of the carbon, but may decrease its performance when the adsorbate is at low concentrations by increasing the mean micropore width.
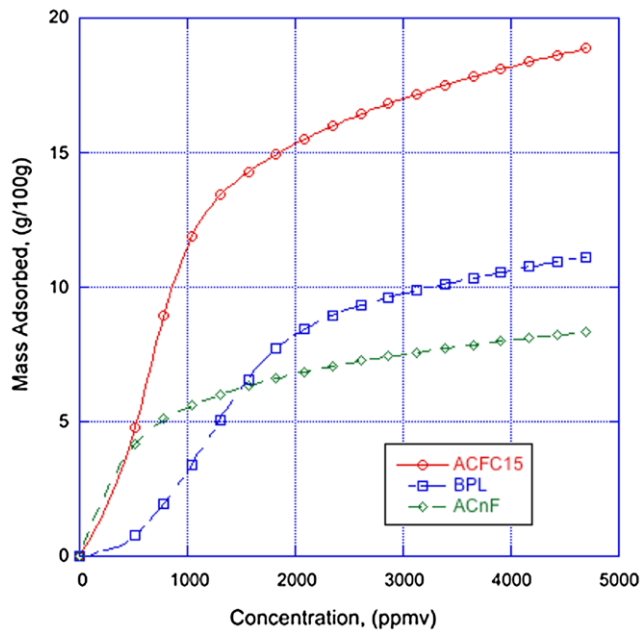
Fig. 5 *n*-Butane adsorption at 25 °C onto ACnF, ACFC, and BPL™

Fig. 6 Water vapor adsorption at 25 °C onto ACnF, ACFC, and BPL

The traditional Type-V water adsorption isotherm is quite apparent for ACFC and BPL™, but less apparent for ACnF, likely due to increased surface polarity resulting from nitrogen or oxygen surface functional groups (Fig. 6). This behavior of ACnF during water adsorption is similar to the behavior of oxidized ACFC (Sullivan et al. 2007) in which case the less prominent hysteresis loop and the uptake of water vapor at lower relative humidity values were attributed to the surface oxygen functional groups. The likelihood of water vapor adsorption by ACnF at low relative humidity values could induce competitive adsorption between the adsorbate of interest (e.g., CWAs, TICs) and water vapor, decreasing the material's overall capacity for the desired adsorbate.

ACnF's high concentration of basic surface functional groups, primarily present from the high nitrogen concentration but possibly also resulting from basic oxygen functionalities (e.g., carbonyl and quinone groups), and in spite of its relatively low pore volume, results in enhanced adsorption of acidic or acid-producing gases compared to ACFC and BPL™. SO_2 adsorption onto ACnF is 2–5 times greater (Fig. 7), and HCN adsorption is 4–20 times greater (Fig. 8), than onto the reference carbons. Adsorption is fully reversible for HCN at room temperature as evidenced by coincident adsorption/desorption isotherms (Fig. 8). Complete regeneration of ACnF is also attained for SO_2. Although the adsorption/desorption isotherms (Fig. 7) do not coincide, upon heating to 200 °C, the ACnF returns to its original mass. The data shown in Figs. 7 and 8 represent a periodic state reached after eight heating/isotherm cycles.

Basic functional groups on the surface of ACnF increase its capacity for SO_2 through adsorption. The significant presence of nitrogen groups (∼10 % N by mass)
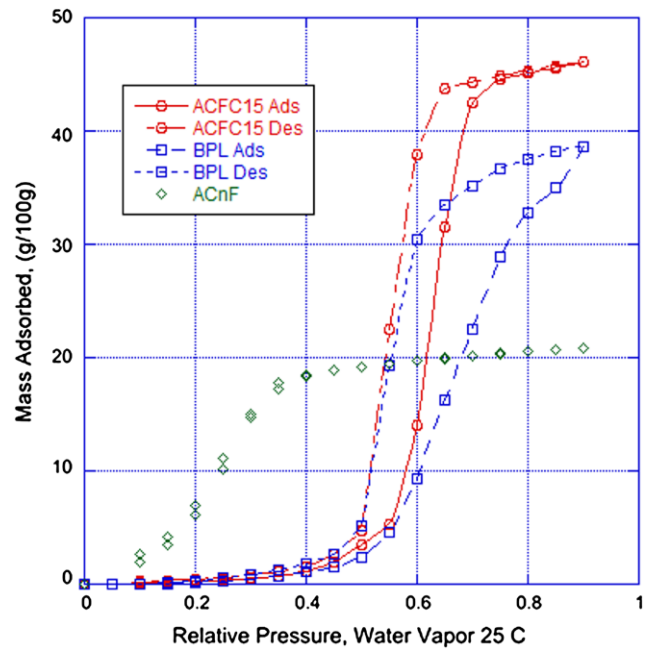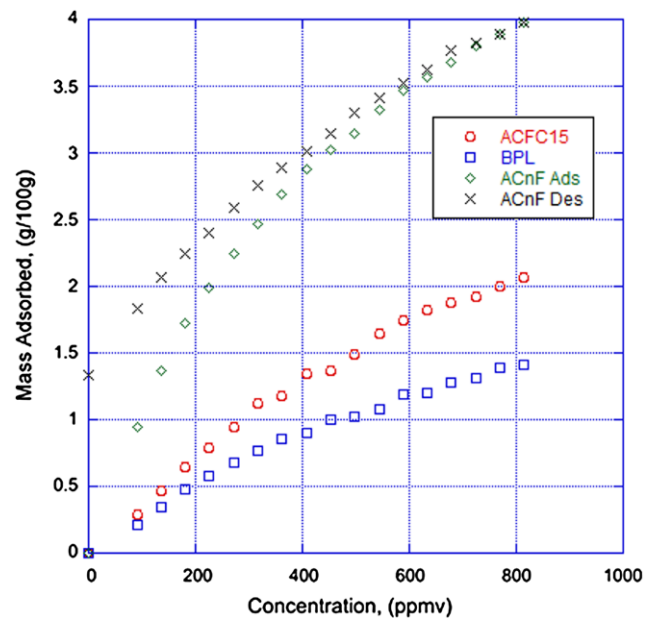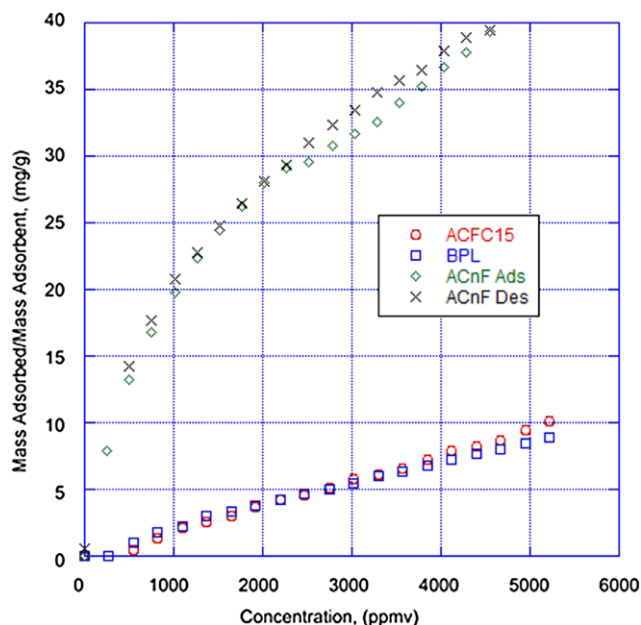

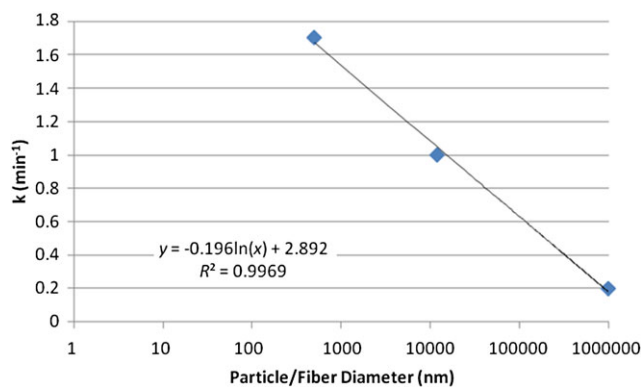Fig. 7 Dry SO_2 adsorption at 25 °C onto ACnF, ACFC, and BPL

on the ACnF surface explains its high capacity for SO_2 compared to ACFC and BPL™ (Mangun et al. 2001b; Raymundo-Pinero et al. 2003). Previous research suggests that pyridinic functionalities on activated carbon linearly impact that adsorbent's ability to oxidize SO_2 to SO_3, which, in turn, increases the SO_2 adsorption capacity of the carbon (Raymundo-Pinero et al. 2003). Despite the fact that ACnF contains nearly twice as many pyrrolic groups as pyridinic groups, the impact of the basic nitrogen species on the car-

Fig. 8 HCN adsorption at 25 °C onto ACnF, BPL™, and ACFC

Fig. 9 Sorption coefficients for ethane adsorption at 25 °C onto ACnF, ACFC, and BPL™ versus particle or fiber diameter (log scale)

bon's SO_2 adsorption capacity is evident. It has been shown previously that for CO_2-activated, PAN-based carbons impregnated with additional nitrogen post activation (using excess solution impregnation techniques), SO_2 adsorption capacity is maximized for materials containing 10 wt% N (Song et al. 2008). A significant advantage of ACnF, therefore, is that the nanofibers contain this ideal amount of nitrogen in their *as-produced* state, ideally saving time, energy, and materials in production of carbon-based SO_2 adsorbents. While ACnF contains a significant amount of nitrogen for adsorption and removal of SO_2, its overall adsorption capacity for SO_2 in dry nitrogen is lower than that of other carbon materials reported in the literature (Davini 1990; Song et al. 2008). The presence of acidic oxygen functionalities, as well as the low micropore volume of the ACnF material (Davini 1990) may be limiting the capacity of ACnF for SO_2. Removal of SO_2 by ACnF may be increased in the presence of O_2 and H_2O, which encourages formation of SO_3 and subsequent hydration to form H_2SO_4 (Mangun et al. 2001b; Davini 2003).

It is useful to compare the HCN adsorption capacity of ACnF (Fig. 8) with results provided by Seredych (Seredych et al. 2009). These HCN adsorption results were obtained at 606,000 ppm_v compared to HCN concentrations reported here, from 0 to 5,200 ppm_v. Lower inlet concentrations of HCN were used in this work to understand the influence of surface functional groups at gas-phase concentrations of HCN that could be expected for human exposure from an atmospheric release, and because HCN's LC_{50} ranges from 135 to 3,404 ppm_v, for exposure times ranging from 30 minutes to 1 minute, respectively (Hathaway et al. 1991). In both studies, the addition of basic surface functional groups

resulted in an increase in HCN adsorption. At the higher concentration used by Seredych et al., capillary condensation is expected even in the untreated carbon, so the relative impact of the surface functional groups on the treated carbon is not as evident. At the lower concentrations used here, the presence of the surface functional groups results in an order-of-magnitude increase in HCN capture over the BPL™ and ACFC reference adsorbents. The adsorption capacity of ACnF for HCN of 27 mg/g (at 2,000 ppm_v, 25 °C) is comparable to the amount of HCN retained (10–50 mg/g) by copper and chromium impregnated activated carbon cloths (Brown et al. 1989). This capacity is considered to be of the order of magnitude necessary for practical application in respiratory devices. For example: assuming a 2,000 ppm_v HCN challenge, 30 liter per minute breathing rate, 80 % bed utilization, and an adsorbent mass of 150 g, a respirator constructed with ACnF would provide ∼48 minutes of protection.

3.3 Adsorption kinetics

Rates of ethane adsorption for ACnF are nearly twice that of ACFC and five times faster than BPL™ (Fig. 9). Nano-dimensioned fibers of ACnF with a high external-surface–to- volume ratio likely facilitate both internal and external mass transfer. Internal mass transfer times may be reduced since the mean distance the adsorbate must travel is shorter. The high external surface area provides better access to the adsorbent's internal micropores. Comparing the three adsorbents, the overall mass transfer appears to increase exponentially (note the log scale in Fig. 9) with decreasing characteristic dimension of the particle/fiber.

The fast kinetics observed for ACnF are advantageous for adsorption processes in general, and can result in improved adsorbent utilization. An example of an ideal application for this material would be as a polishing adsorbent layer in a respirator. These fast kinetics are also particularly advantageous in cyclic processes such as pressure-swing adsorption

systems, where the minimum adsorption cycle time determines the overall size (and cost) of the system.

4 Summary

Activated Carbon nanoFiber (ACnF) is a carbon-based, nano-scale adsorbent with unique properties. The low total pore volume, narrow pore width, and high nitrogen content of ACnF indicate a low degree of activation for this material compared to commercially available activated carbon fiber cloth and BPL™ granular activated carbon, which are considered here as reference adsorbents. The low micropore volume and surface area of ACnF result in reduced total capacity for hydrocarbons through physical adsorption at high concentrations. However, at low concentrations (<500 ppm$_v$), the narrow mean pore width (0.72 nm) results in similar capacity for hydrocarbons as ACFC and about three times higher than Calgon BPL™. Although the nitrogen in the structure ($\sim$10 % by mass) makes the ACnF more hydrophilic, it also gives this material up to 20 times better adsorption capacity for acidic toxic industrial chemicals (TICs), including HCN and SO_2. The enhanced adsorption capacity for these acidic and acid producing TICs was shown to be reversible. The nanofiber morphology results in faster adsorption kinetics compared to the two reference adsorbents because the ACnF's internal micropores are more accessible to the adsorbate. ACnF's properties may facilitate the development of improved air purification devices such as less restrictive and better performing respirators, regenerative filter systems that can protect against TICs, or perhaps smaller and more energy-efficient pressure-swing-adsorption systems.

References

Azizian, S.: Kinetic models of sorption: a theoretical analysis. J. Colloid Interface Sci. **276**(1), 47–52 (2004)

Bagreev, A., Bashkova, S., et al.: Adsorption of SO_2 on activated carbons: the effect of nitrogen functionality and pore sizes. Langmuir **18**(4), 1257–1264 (2002)

Bansal, R.C., Goyal, M.: Activated carbon modification by impregnation. In: Activated Carbon Adsorption, pp. 58–60. CRC, Boca Raton (2005)

Boudou, J.P.: Surface chemistry of a viscose-based activated carbon cloth modified by treatment with ammonia and steam. Carbon **41**(10), 1955–1963 (2003)

Boudou, J.P., Chehimi, M., et al.: Adsorption of H_2S or SO_2 on an activated carbon cloth modified by ammonia treatment. Carbon **41**(10), 1999–2007 (2003)

Brown, P.N., Jayson, G.G., et al.: Effect of aging and moisture on the retention of hydrogen cyanide by impregnated activated charcoals. Carbon **27**(6), 821–833 (1989)

Calvete, T., Lima, E.C., et al.: Application of carbon adsorbents prepared from the Brazilian pine-fruit-shell for the removal of Procion Red MX 3B from aqueous solution—kinetic, equilibrium, and thermodynamic studies. Chem. Eng. J. **155**(3), 627–636 (2009)

Chiang, Y.C., Lee, C.Y., et al.: Surface chemistry of polyacrylonitrile- and rayon-based activated carbon fibers after post-heat treatment. Mater. Chem. Phys. **101**(1), 199–210 (2007)

Davini, P.: Adsorption and desorption of SO_2 on active-carbon—the effect of surface basic groups. Carbon **28**(4), 565–571 (1990)

Davini, P.: Flue gas desulphurization by activated carbon fibers obtained from polyacrylonitrile by-product. Carbon **41**(2), 277–284 (2003)

Economy, J., Mangun, C.: Novel fibrous systems for contaminant removal. In: Pawliszyn, J. (ed.) Sampling and Sample Preparation for Field and Laboratory. Elsevier, Amsterdam (2002). Ch. 31

Evans, M.J.B., Halliop, E., et al.: The effect of chlorination on surface properties of activated carbon. Carbon **36**(11), 1677–1682 (1998)

Hathaway, G.J., Proctor, N.H., et al.: Proctor and Hughes' Chemical Hazards of the Workplace. Van Nostrand Reinhold, New York (1991)

Ko, T.H., Chiranairadul, P., et al.: The effects of activation by carbon dioxide on the mechanical properties and structure of PAN-based activated carbon fibers. Carbon **30**(4), 647–655 (1992)

Kundu, S., Xia, W., et al.: The formation of nitrogen-containing functional groups on carbon nanotube surfaces: a quantitative XPS and TPD study. Phys. Chem. Chem. Phys. **12**(17), 4351–4359 (2010)

Luo, L., Ramirez, D., et al.: Adsorption and electrothermal desorption of organic vapors using activated carbon adsorbents with novel morphologies. Carbon **44**(13), 2715–2723 (2006)

Mangun, C.L., Braatz, R.D., et al.: Fixed bed adsorption of acetone and ammonia onto oxidized activated carbon fibers. Ind. Eng. Chem. Res. **38**(9), 3499–3504 (1999)

Mangun, C.L., Benak, K.R., et al.: Surface chemistry, pore sizes and adsorption properties of activated carbon fibers and precursors treated with ammonia. Carbon **39**(12), 1809–1820 (2001a)

Mangun, C.L., Debarr, J.A., et al.: Adsorption of sulfur dioxide on ammonia-treated activated carbon fibers. Carbon **39**(11), 1689–1696 (2001b)

Nakayama, A., Suzuki, K., et al.: Electronic and magnetic properties of activated carbon fibers. Bull. Chem. Soc. Jpn. **69**(2), 333–339 (1996)

Pereira, M.F.R., Soares, S.F., et al.: Adsorption of dyes on activated carbons: influence of surface chemical groups. Carbon **41**(4), 811–821 (2003)

Peterson, G.W., Karwacki, C.: Novel collective protection filters for emerging TIC requirements: axial- and radial-flow filter designs. Edgewood Chemical and Biological Center. ECBC-TR-497 (2007)

Pradhan, B.K., Sandle, N.K.: Effect of different oxidizing agent treatments on the surface properties of activated carbons. Carbon **37**(8), 1323–1332 (1999)

Ramirez, D., Sullivan, P.D., et al.: Equilibrium adsorption of organic vapors on phenol-, tire-, and coal-derived activated carbons. J. Environ. Eng. **130**(3), 231–241 (2004)

Raymundo-Pinero, E., Cazorla-Amoros, D., et al.: The role of different nitrogen functional groups on the removal of SO_2 from flue gases

by N-doped activated carbon powders and fibres. Carbon **41**(10), 1925–1932 (2003)

Rivera-Utrilla, J., Sanchez-Polo, M., et al.: Activated carbon modifications to enhance its water treatment applications. an overview. J. Hazard. Mater. **187**(1–3), 1–23 (2011)

Rodriguez-Reinoso, F.: The role of carbon materials in heterogeneous catalysis. Carbon **36**(3), 159–175 (1998)

Ryu, Z.Y., Rong, H.Q., et al.: Microstructure and chemical analysis of PAN-based activated carbon fibers prepared by different activation methods. Carbon **40**(7), 1144–1147 (2002)

Saysset, S.: Procédé d'adsorption sur adsorbant carboné avec régénération thermique par effet joule direct: application au traitement d'effluents chargés en composés organiques volatils. L'Institut National Polytechnique de Lorraine, Doctoral Thesis (Dec. 1999). 1999

Seredych, M., van der Merwe, M., et al.: Effects of surface chemistry on the reactive adsorption of hydrogen cyanide on activated carbons. Carbon **47**(10), 2456–2465 (2009)

Song, X., Wang, Z., et al.: Ultrafine porous carbon fibers for SO_2 adsorption via electrospinning of polyacrylonitrile solution. J. Colloid Interface Sci. **327**(2), 388–392 (2008)

Stohr, B., Boehm, H.P., et al.: Enhancement of the catalytic activity of activated carbons in oxidation reactions by thermal treatment with ammonia or hydrogen-cyanide and observation of a superoxide species as a possible intermediate. Carbon **29**(6), 707–720 (1991)

Subrenat, A., Baleo, J.N., et al.: Electrical behaviour of activated carbon cloth heated by the joule effect: desorption application. Carbon **39**(5), 707–716 (2001)

Sullivan, P.D., Rood, M.J., et al.: Adsorption and electrothermal desorption of hazardous organic vapors. J. Environ. Eng. **127**(3), 217–223 (2001)

Sullivan, P.D., Stone, B.R., et al.: Water adsorption with hysteresis effect onto microporous activated carbon fabrics. Adsorption **13**(3–4), 173–189 (2007)

Sun, J., Chen, S., et al.: Correlating N_2 and CH_4 adsorption on microporous carbon using a new analytical model. Energy Fuels **12**(6), 1071–1078 (1998)

Vora, M.: Personal Communication on Processing ACnF. P. D, Sullivan (2009)

Wang, P.H., Yue, Z.R., et al.: Conversion of polyacrylonitrile fibers to activated carbon fibers: effect of activation. J. Appl. Polym. Sci. **60**(7), 923–929 (1996)

Weitz, R., Al-Marashi, I., et al.: Chlorine as a terrorist weapon in Iraq. WMD Insights. www.wmdinsights.org/I15/I15_ME1_chlorine.htm (2007)

Wu, Z.H., Sugimoto, Y., et al.: Formation of N_2 from pyrrolic and pyridinic nitrogen during pyrolysis of nitrogen-containing model coals. Energy Fuels **17**(3), 694–698 (2003)

Yue, Z.R., Mangun, C.L., et al.: Preparation of fibrous porous materials by chemical activation 1. $ZnCl_2$ activation of polymer-coated fibers. Carbon **40**(8), 1181–1191 (2002)